Calculation of alpha particle redistribution in sawteeth using experimentally reconstructed displacement eigenfunctions

R. Farengo[1], H. E. Ferrari[1,2], M.-C. Firpo[3], P. L. Garcia-Martinez[2,3], A. F. Lifschitz[4]
[1]Comisión Nacional de Energía Atómica,
Centro Atómico Bariloche, Bariloche, Argentina
[2]CONICET, Bariloche, Argentina
[3]Laboratoire de Physique des Plasmas, Ecole Polytechnique, Palaiseau, France
[4]Laboratoire de Physique des Gaz et des Plasmas,
Universite Paris Sud, Orsay, France

1 Introduction

The dynamics of alpha particles will be extremely important in ITER and future fusion reactors. Sawtooth oscillations can produce a redistribution of the alpha particle population, thus modifying the power deposition profile and increasing alpha particle losses and wall loading. In addition, alpha particle transport from the core to the outer region can trigger other instabilities.

Most previous studies of the effect of sawtooth crashes on alpha particle confinement have employed a phenomenological description of the evolution of the magnetic flux surfaces during a sawtooth and included only the dominant (1,1) kink mode. Initial studies assumed that the particles were tied to the flux surfaces, and moved with them [1]. Later, the importance of the electric field associated to the kink modes was recognized and incorporated in the calculations [2]. These studies are useful to qualitatively understand the effect of the perturbation on different groups of particles and the general evolution of the process but can not be used to make quantitative calculations of the energy and particle fluxes in future fusion reactors.

Our method consist on calculating the exact alpha particle trajectories in the total electric and magnetic fields (equilibrium plus perturbation). Knowing the trajectories, the particle and energy fluxes can be easily calculated. A similar approach was employed by Zhao and White [3] but, as will be shown below, our method includes some important differences regarding the calculation of the total fields and the particle orbits. In principle, the total fields could be calculated by numerically solving the nonlinear 3D resistive MHD equations. It is well known, however, that the results obtained with the "classical" resistive MHD equations do not reproduce the experimental observations. A significant effort is currently underway to include additional effects (energetic particles, Hall term, etc.) in the codes to obtain a better agreement with the experiments but the results are as yet not completely satisfactory. Our approach is to directly incorporate the experimental information in a simple, ideal MHD, model. The most important features of the method can be summarized as follows:

1. The information regarding the space and time dependence of the perturbation is taken from the experimental results published in Ref. [4]. We believe this is the most important feature of our model because it allows us to study the evolution of the alpha particles in the presence of the experimentally determined perturbations.

2. The exact trajectories are calculated, no guiding center approximation is employed. Although this requires significantly larger computational resources we believe it is justified because the width of the orbits can be larger than the typical scale length of the mode structure.

The main purpose of this first study is to introduce the method and present its basic features and capabilities. Future work will be devoted to study specific aspects and to calculate the global energy and particle transport induced by the sawteeth.

The structure of this paper is as follows. In Sec. 2 we describe the analytical equilibrium employed and in Sec. 3 the method used to calculate the perturbed electric and magnetic fields. Section 4 contains a brief description of the numerical techniques employed and Sec. 5 the results of the numerical calculations. Finally, is Sec. 6 we summarize our findings and discuss future research on this topic.

2 Equilibrium

A simple analytical model is employed to calculate the equilibrium magnetic field. The Grad-Shafranov equation is expanded in powers of the inverse aspect ratio (ε) and only the first two terms (ε^0 and ε^1) are included in the solution. In toroidal coordinates we have:

$$\psi(x,\phi) = \psi_0(x) + \varepsilon\psi_1(x,\phi) \tag{1}$$

where ψ is the poloidal flux, x the normalized minor radius ($x = \rho/a$) and ϕ the poloidal angle. We normalize the poloidal flux with $B_0\pi a^2$, where B_0 is the external toroidal field at the geometric axis (R_0), and assume that the pressure and poloidal current depend on the normalized poloidal flux as:

$$p = p_1\psi^2; \qquad I^2 = I_0^2 + I_1^2\psi^2 \tag{2}$$

where p is normalized with $B_0^2/8\pi$ and I with $B_0 c R_0/2$ (Gaussian units are employed). Substituting this in the Grad-Shafranov equation we obtain:

$$\psi_0(x) = CJ_0(kx), \qquad \psi_1(x,\phi) = \frac{\cos\phi}{2}\left\{C\left[xJ_0(kx) - \frac{\sigma x^2}{k}J_1(kx)\right] - DJ_1(kx)\right\} \tag{3}$$

where $J_0(kx)$ and $J_1(kx)$ are Bessel functions, $\sigma = 4p_1/\varepsilon^2$ and $k^2 = 4(p_1+I_1^2)/\varepsilon^2$. The boundary of the plasma is at the $x = 1$ surface, where we request the flux to be zero. Then, we have $\psi_0(1) = 0$, $\psi_1(1,\phi) = 0$ and therefore k has to be a zero of J_0 and $D = \sigma C/k$. The constant C is determined by fixing the poloidal field at the plasma boundary (total toroidal plasma current) and I_0 is related to the vacuum toroidal field. Since we normalize all the fields with the vacuum toroidal field at R_0, $I_0 = 1$. Finally, σ, which is proportional to p_1, fixes the plasma β. Knowing the poloidal flux we can calculate the equilibrium magnetic field.

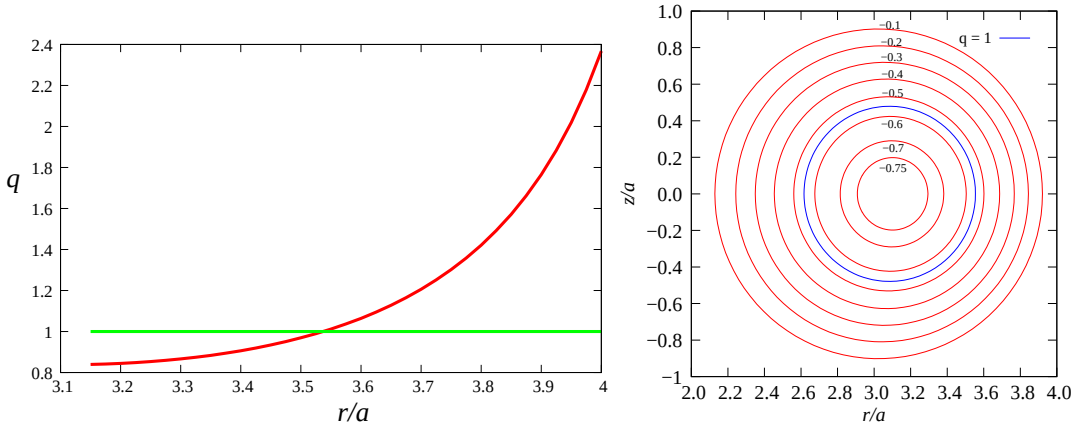

Figure 1: q profile and flux surfaces of the equilibrium employed

The simple analytical equilibrium introduced above does not provide much flexibility to control the shape of the safety factor profile, which is critical for the onset of the instability. We have

chosen a set of parameters ($\varepsilon = 1/3$, $p_1 = 0.05$, $B_{pol}(x = 1, \phi = 0) = 0.155$) that give a low enough q value at the magnetic axis ($q_0 = 0.85$), without moving the $q = 1$ surface too far out. Figure 1 shows the q profile and the flux surfaces obtained with these parameters.

3 Perturbed fields

Reference [4] provides the spatial structure and temporal variation of the displacement eigenfunctions measured in the experiments. We employ this information to calculate the perturbed electric and magnetic fields. The major approximation employed in our model is the use of a "cylindrical", instead of toroidal, displacement eigenfunction. This is justified by the following reasons:

1. The experimental information provided in [4] corresponds to a "cylindrical" mode. The amplitude of the displacement eigenfunction depends only on the minor radius (in toroidal coordinates) and the poloidal and toroidal dependences are included only in the phase (see eq. (2) of [4]).

2. As already noted by Zhao and White [3], the effective aspect ratio of the flux surfaces affected by the sawtooth (inside the $q = 1$ surface) is larger than the aspect ratio of the device (R_0/a).

3. The perturbed fields can be calculated analytically.

We will follow the alpha particle trajectories for times much shorter than the resistive time. We therefore employ ideal MHD to calculate the perturbed magnetic field produced by a known displacement field:

$$\mathbf{B}_1 = \nabla \times (\xi \times \mathbf{B}) \tag{4}$$

where $\mathbf{B}_1$ is the perturbed magnetic field, ξ is the displacement and $\mathbf{B}$ the equilibrium magnetic field calculated above. We note that Eq. (4) means that the perturbed vector potential is perpendicular to the equilibrium magnetic field ($\mathbf{A}_1 = \xi \times \mathbf{B}$). This is different from the assumption used in [3], where $\mathbf{A}_1$ is assumed to be parallel to $\mathbf{B}$. To be consistent with the spatial dependence assumed below for the displacement, only the "cylindrical" part of $\mathbf{B}$ is used to calculate $\mathbf{B}_1$ and $\mathbf{E}_1$ (but the full $\mathbf{B}$ is used to calculate particle orbits).

In this study we include the $(1, 1)$ and $(2, 2)$ modes. Following Ref. [4] we therefore write the x component of the displacement as:

$$\xi_x(x, \phi, \theta, t) = \xi_x^{11}(x, t)\cos(\phi - \theta - \omega t) + \xi_x^{22}(x, t)\cos[2(\phi - \theta - \omega t)] \tag{5}$$

where θ is the toroidal (azimuthal) angle and ω is the frequency of oscillation. Considering incompressible displacements ($\nabla \cdot \xi = \mathbf{0}$) and minimizing the change in potential energy for internal modes we can write the other components of ξ in terms of ξ_x [5].

The electric field is obtained from the ideal Ohm's law:

$$\mathbf{E}_1 = -\frac{\mathbf{v}_1 \times \mathbf{B}}{c} = -\frac{1}{c}\frac{\partial}{\partial t}(\xi \times \mathbf{B}) \tag{6}$$

To proceed we need to specify $\xi_x^{11}(x, t)$ and $\xi_x^{22}(x, t)$, which are taken from the experimental information provided in Fig. 4 (for the x dependence) and Fig. 3 (for the time dependence) of Ref. [4]. Separating the space and time dependence as:

$$\xi_x^{mn}(x, t) = \xi_0^{mn}(t) f^{mn}(x) \tag{7}$$

we introduce the following $f^{mn}(x)$:

$$f^{11}(x) = \frac{1}{2}\{1 - \tanh[\delta(x - x_s)]\}$$

$$f^{22}(x) = \begin{cases} \cos^2\left[\frac{\pi}{2}\left(\frac{x-x_2}{x_2}\right)\right] + \frac{e^{-x^2/x_2^2}}{4}, & x \le x_a \\ 0, \quad x > x_a \end{cases}$$

where x_s is the (minor) radius of the $q = 1$ surface, $x_2 \simeq 0.35$, $f^{22}(x_a) = 0$ and δ is a numerical constant adjusted to get the desired slope of the $(1,1)$ eigenfuction at $x = x_s$ (typically $\delta \gtrsim 20$).

The results obtained in [4] show that the $(1,1)$ mode survives the crash and slowly decays after it. It is also shown that by the time the $(2,2)$ mode begins to grow, the $(1,1)$ mode already has an amplitude which is approximately 70 % of its maximum value (see Fig. 3 in [4]). In most of our simulations we follow the particles from the time the $(2,2)$ mode begins to grow, go through the crash and continue until the $(2,2)$ mode has disappeared and the $(1,1)$ has returned to its initial amplitude. The method employed to specify the temporal dependence of the amplitude of the modes is similar to the one employed in [3] but our time dependent functions are more complicated due to the existence of two modes with different grow and decay rates. The explicit time dependences employed are:

Growth phase

$$\begin{aligned} \xi_0^{11}(t) &= \xi_0^{11}\left[c_1 + \frac{\exp\{t/(c_2 t_c)\} - 1}{e-1}\right], \quad 0 < t \le t_c \\ \xi_0^{22}(t) &= \xi_0^{22}\frac{[\exp\{t/t_c\} - 1]}{e-1}, \quad 0 < t \le t_c \end{aligned}$$

where t_c is the crash time and c_1 and c_2 are numerical constants, chosen to obtain the desired amplitudes at $t = 0$ and $t = t_c$. Setting $c_1 = 0.7$ and $c_2 = 2.4054$, the amplitude of the $(1,1)$ mode is $0.7\xi_0^{11}$ at $t = 0$ and ξ_0^{11} at $t = t_c$. The $(2,2)$ mode begins to grow at $t = 0$ and reaches its maximum value at $t = t_c$. According to Fig. 3 of [4], the $(2,2)$ mode begins to grow approximately $1.5 \times 10^{-3}s$ before the crash; we therefore set $t_c = 1.5 \times 10^{-3}s$.

Decay phase

$$\begin{aligned} \xi_0^{11}(t) &= \xi_0^{11}\left\{c_1 + \frac{(1-c_1)}{e-1}\left[\exp\{(t_c + t_{11} - t)/t_{11}\} - 1\right]\right\}, \quad t_c < t \le t_c + t_{11} \\ \xi_0^{22}(t) &= \xi_0^{22}\frac{[\exp\{(t_c + t_{22} - t)/t_{22}\} - 1]}{e-1}, \quad t_c < t \le t_c + t_{22} \end{aligned}$$

where t_{11} is the time (after the crash) it takes the $(1,1)$ mode to return to its initial amplitude ($0.7\xi_0^{11}$) and t_{22} is the time it takes the $(2,2)$ mode to vanish. In general we have taken $t_{11} = t_c$ and $t_{22} = t_c/5$. Although laborious, this method can be used to introduce a time dependence that matches the experimental observations.

4 Numerical methods

A low dissipation, fourth order, Runge-Kutta method [6] is employed to calculate the exact particle trajectories in the time dependent fields. Collisions are not included because the simulation time is much shorter than the collision time. The time step is taken small enough to guarantee that, when the perturbed electric field is not included, the energy and azimuthal (toroidal) component of the canonical momentum (P_θ) are conserved (error less than 1%). The initial conditions for each particle are determined using the following procedure:

1. The flux surface were the particle is initially located is chosen by fixing the poloidal flux (ψ_0).

2. A random value is chosen for the poloidal angle (ϕ_0). Having ψ_0 and ϕ_0 the initial values of r and z are calculated.

3. The energy of the particle (absolute value of the initial velocity) is fixed ($E_0 \leq 3.5\ MeV$) and a random (isotropic) initial direction is chosen.

In the equations of motion the time is normalized with the cyclotron frequency of an alpha particle in the external toroidal field at the geometric axis (Ω_α), lengths are normalized with the minor radius (a) and velocities with the initial velocity of the alpha particle (v_0). This results in a single dimensionless parameter appearing in the normalized equations:

$$\gamma = \frac{v_0}{\Omega_\alpha a}$$

With ITER like parameters ($B_0 = 5.3T$, $a = 2\ m$), $\gamma = 2.552 \times 10^{-2}$ for a 3.5 MeV alpha particle and decreases as the square root of the energy for lower energies.

5 Results

The interaction between the alpha particles and the perturbation depends on the relationship between the mode frequency and the frequencies associated to periodic particle motions. The bouncing of trapped particles, their toroidal precession and the toroidal and poloidal rotation of passing particles are examples of such periodic motions. Since particles are distributed in flux surfaces with random pitch angle their periods are different. It is possible, however, to obtain

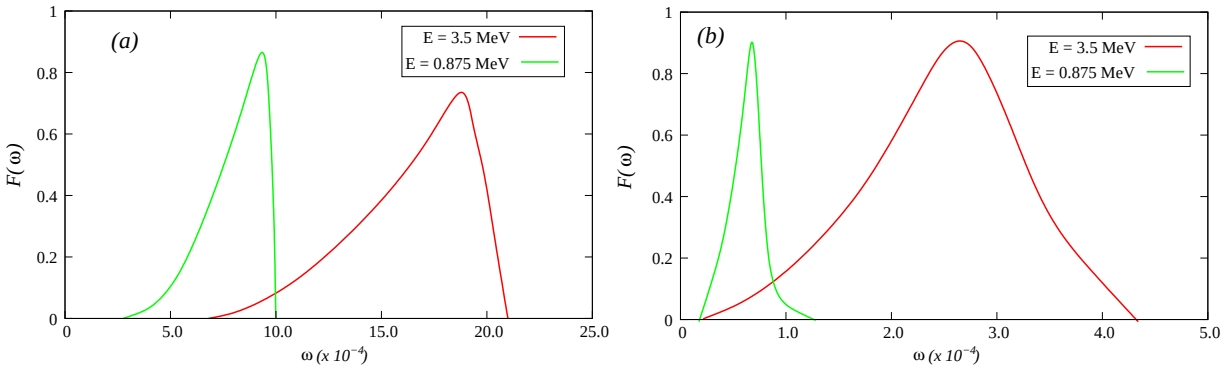

Figure 2: *(a)*Distribution function of the bounce frequency of 3.5 MeV and 0.875 MeV trapped particles initially located at the $\psi = -0.7$ flux surface ($q = 0.89$).*(b)*Distribution function of the precession frequency of 3.5 MeV and 0.875 MeV trapped particles initially located at the $\psi = -0.7$ flux surface ($q = 0.89$)

information about the average frequencies, and their distribution, by constructing a frequency distribution function F(ω) for the different periodic motions. Figure 2 *(a)*, shows F(ω) for the bounce motion of 3.5 MeV and 0.875 MeV trapped particles initially located at the $\psi = -0.7$ flux surface ($q = 0.89$). Clear maxima are observed at $\omega = 18.9 \times 10^{-4}$, for 3.5 MeV particles and at $\omega = 9.4 \times 10^{-4}$, for 0.875 MeV particles. As expected, the ratio between the frequencies corresponding to the maxima is 2 (the ratio of the energies is 4). The plots show a fast decay on the high frequency side of the maxima and a longer tail on the low frequency side. Figure. 2 *(b)* shows plots of F(ω) for the precession motion of trapped particles for the same values of energy as in Fig. 2 *(a)*. Well defined maxima are observed at $\omega = 2.74 \times 10^{-4}$, for 3.5 MeV particles and at $\omega = 7.39 \times 10^{-5}$, for 0.875 MeV particles. Since the precession frequency depends on the particle energy the ratio of the frequencies corresponding to the two maxima is 4 in this case. Finally, in Fig. 3, we show a plot of F(ω) for the toroidal rotation of passing particles with the same energies as above. As expected, the ratio of the frequencies corresponding to the maxima is 2. The period of poloidal rotation will be similar to the period of toroidal rotation because the particles are initially located at flux surfaces with $q \simeq 1$. Since the parameters

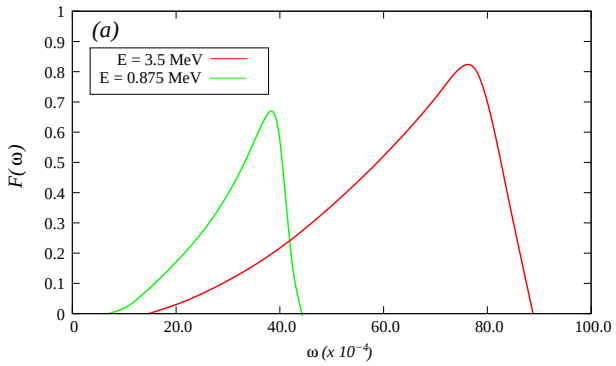

Figure 3: Distribution function of the toroidal frequency of 3.5 MeV and 0.875 MeV passing particles initially located at the $\psi = -0.7$ flux surface ($q = 0.89$)

of our equilibrium are similar to those of ITER (except for the elongation) the frequencies of periodic alpha particle motion in ITER should be similar to those shown in the plots presented above (probably lower frequency for the trapped particles due to the higher elongation).

The distance from a point (r, z) on a flux surface to the magnetic axis is given by:

$$y = \left[(r - R_a)^2 + z^2\right]^{1/2}$$

where R_a is the radial position of the magnetic axis in cylindrical coordinates. Perfectly circular flux surfaces centered at the magnetic axis would have a constant value of y. For our equilibrium this is approximately true. To quantify the displacement of the particles from the flux surfaces we introduce a dimensionless *diffusion* coefficient defined as:

$$D(\psi) = \frac{\left\langle (y_f - y_0)^2 \right\rangle}{\Delta t} \tag{8}$$

where y_f and y_0 are the final and initial values of y and ψ indicates the flux surface where the particles were initially located, Δt is the time interval and $\langle\rangle$ means average over a large number of particles. Note that with this simple definition D is not zero in the absence of perturbations due to the finite Larmor radius and banana width. We will show, however, that in most cases the perturbation increases D well above its unperturbed value.

The frequency measured in Ref. [4] for the $(1, 1)$ mode was approximately $\omega = 5.5 \times 10^4 s^{-1}$, which corresponds to a normalized value of 2.08×10^{-4}. Although not known at this time, the frequency should be significantly lower in ITER. To test our method and the numerical code we have nevertheless explored a higher frequency regime to study the behavior of the diffusion coefficient near the maxima shown in Figs. 2,3 for $3.5MeV$ particles. Figure 4 shows a plot of the diffusion coefficient as a function of the mode frequency for 3.5 MeV particles initially located at the $q = 0.89$ surface when both modes are present ($\xi_0^{11} = 0.06$, $\xi_0^{22} = \xi_0^{11}/3$). Particles have been separated according to their unperturbed behavior in trapped, positive (passing particles that rotate in the same sense as the plasma current) and negative (rotate in the opposite sense). The curves in the plot indicate the diffusion coefficient obtained for each type of particle, weighted with its relative fraction, and the total diffusion coefficient. The value of the total diffusion coefficient for the case without perturbation is shown as a horizontal dashed line. Note that a dimensionless diffusion coefficient of 5×10^{-9} corresponds to an actual value of approximately 5 m^2/s. The trapped particle coefficient presents a low frequency maximum located at approximately the same value as the precession peak shown in Fig. 2*(b)* and a second maximum at a frequency which is lower than the frequency corresponding to the maximum of the bounce frequency (see Fig.2(a)). The maxima are smooth and have a value which is only

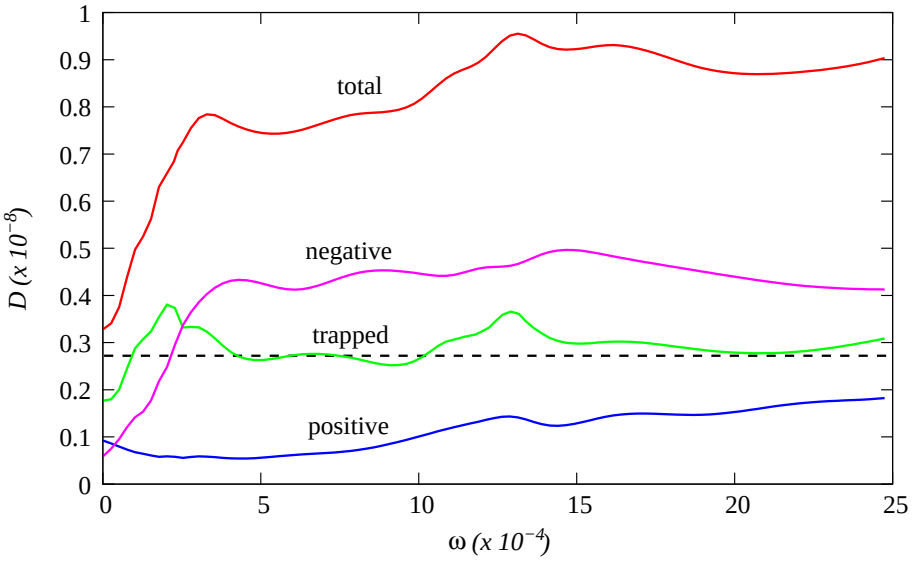

Figure 4: Diffusion coefficient as a function of the mode frequency for 3.5 MeV particles initially located at the $q = 0.89$. Dashed line represents the diffusion coefficient value without perturbation.

30-40% higher than the values obtained at intermediate frequencies. The displacement of the bouncing peak towards lower frequencies can be partially justified by noting the asymmetric shape of the bounce frequency peak in Fig. 2, which has a long tail in the low frequency side. Negative passing particles have a large, and fairly constant, diffusion coefficient for frequencies above 3×10^{-4} while positive particles have a very small diffusion coefficient. The difference between positive and negative passing particles stems from the signs used in the terms appearing in the phase of the mode. With our definitions the mode propagates in the negative sense.

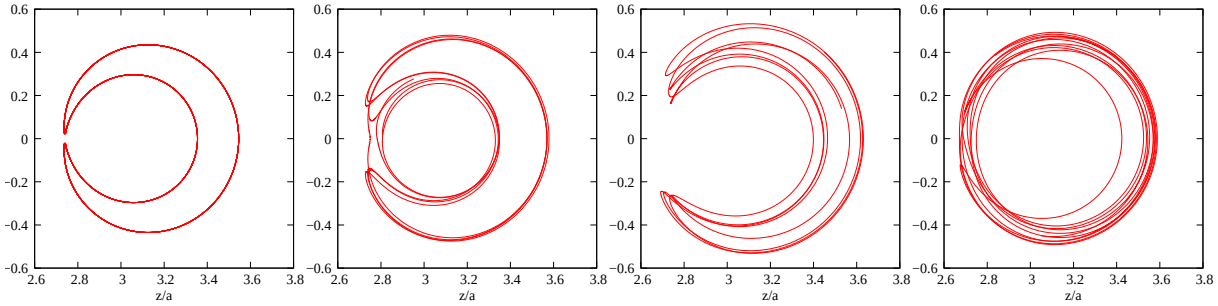

Figure 5: Part of the orbit (the instantaneous position of the guiding center) of an initially trapped particle perturbed by a mode with $\omega = 2 \times 10^{-3}$.

The analysis presented above, where the maxima of the diffusion coefficient are related to the frequencies of the periodic motions of unperturbed particles is oversimplified. Once the perturbation begins to grow, particle orbits can change significantly, switching from trapped to passing, or viceversa, many times during the simulation. This is shown in Fig. 5 which shows part of the orbit (the instantaneous position of the guiding center) of an initially trapped particle perturbed by a mode with $\omega = 2 \times 10^{-3}$ (close to the bouncing peak). Fig. 6 shows the temporal evolution of the parallel velocity for the same particle. The changes from trapped to passing, back to trapped, etc. are evident. Although not shown here the same type of behavior can be found in initially passing particles.

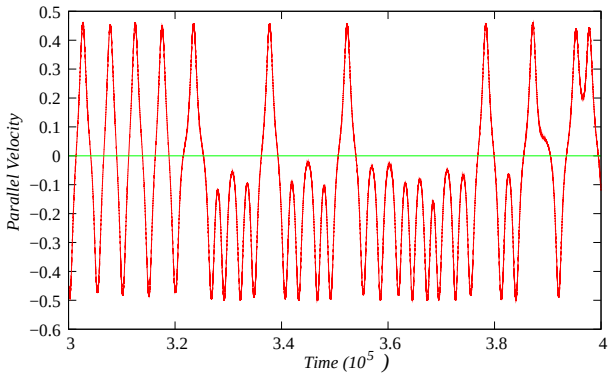

Figure 6: Temporal evolution of the parallel velocity for the particle of Fig. 5.

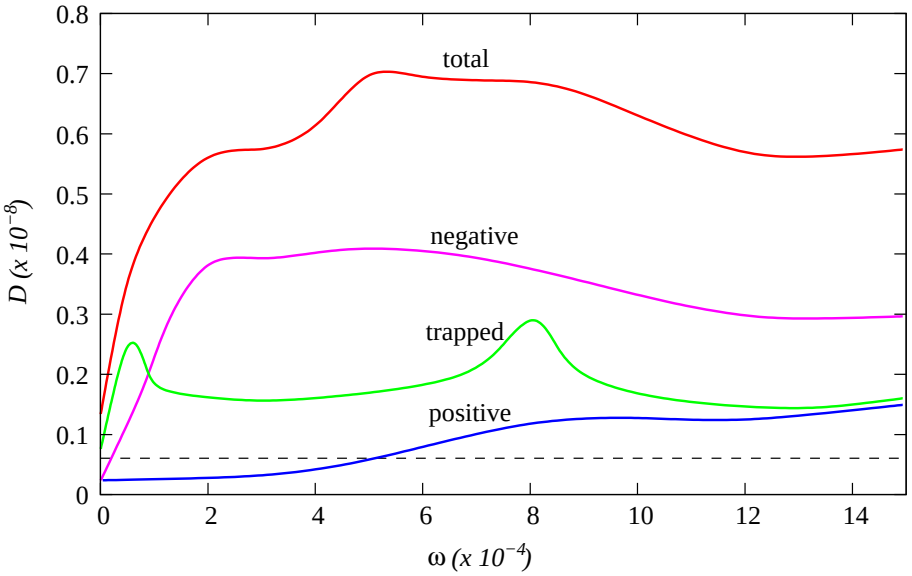

Figure 7: Diffusion coefficient as a function of the mode frequency for 0.875 MeV particles initially located at the $q = 0.89$. Dashed line represents the diffusion coefficient value without perturbation.

Figure 7 shows the diffusion coefficient as a function of the mode frequency for particles with $E = 0.875\ MeV$ initially located at the $q = 0.89$ surface. Clear peaks can be observed in the trapped particles diffusion coefficient at the precession and bounce frequencies. Although not very clear from the plots the diffusion coefficient of 0.875 MeV particles becomes larger than the coefficient of 3.5 MeV particles at frequencies below 0.5×10^{-4}. This is consistent with the idea that sawteeth will be usefull to remove helium ashes.

The effect of including only the $(1, 1)$ mode, eliminating the perturbed electric field and changing the amplitude of the perturbation has also been investigated. Table 1 summarizes the diffusion coefficient (multiplied by 10^9) obtained for three typical frequency values. Case A has no perturbation; it corresponds to the "natural" width of particle orbits. Case B has both modes, with $\xi_0^{11} = 0.06$, $\xi_0^{22} = \xi_0^{11}/3$ (as above). In case C the $(2, 2)$ mode was eliminated while in case D the electric field was eliminated. Finally, case E is like case B but with $\xi_0^{11} = 0.12$. The effect of eliminating the (2,2) mode is relatively small, and increases with the frequency. Eliminating the electric field produces a significant reduction in the diffusion coefficient, which is larger at higher frequencies. Note that the electric field increases with the frequency, and so does the diffusion coefficient calculated with $\mathbf{E}_1$. However, the diffusion coefficient calculated

	$\omega = 0.5 \times 10^{-4}$	$\omega = 2 \times 10^{-4}$	$\omega = 13 \times 10^{-4}$
A	2.712	2.712	2.712
B	3.719	6.801	9.539
C	3.594	6.390	8.274
D	3.424	4.513	4.066
E	4.702	9.973	20.261

Table 1: Summary of results obtained for different conditions.

without $\mathbf{E}_1$ is larger at $\omega = 2 \times 10^{-4}$ than at $\omega = 13 \times 10^{-4}$. Increasing the amplitude of the perturbation also has an effect that increases with frequency.

6 Summary

We presented a method to calculate the effect of sawtooth oscillations on alpha particle confinement using the experimental information available. A relatively simple analytical procedure was used to calculate the perturbed electric and magnetic fields produced by low order, internal kink modes. The exact trajectories of a large number of alpha particles in the total (equilibrium plus perturbation) fields were calculated and a diffusion coefficient was introduced to quantify the magnitude of the displacement from the initial flux surface produced by the perturbation.

We showed that although some features of the behavior of the alpha particles can be explained in terms of simple mode particle resonances the situation can be significantly more complicated.

In the studies presented above we considered monoenergetic particles distributed over a single flux surface. In future studies we will consider the entire plasma volume inside the $q = 1$ surface with the energy of the particles distributed according to the expected slowing down distribution. This will allow the calculation of the total energy and particle fluxes produced by the sawtooth.

Acknowledgement

Financial support from the ECOS-MINCyT Research Grant No. A09E02 is gratefully acknowledged.

References

[1] Y. I. Kolesnichenko, Yu. V. Yakovenko, *Nucl. Fusion* **36**, 159 (1996).

[2] Y. I. Kolesnichenko, V. V. Lutsenko, R. B. White, Yu. V. Yakovenko, *Nucl. Fusion* **7**, 1325 (2000).

[3] Y. Zhao, R. B. White, Phys. Plasmas **4** (4) (1997).

[4] V. Igochine et al., Nuc. Fusion **47**, 23-32 (2007).

[5] J. P. Freidberg *"Ideal Magneto Hydrodynamics"*, Plenun Press, Chapter 9, (1987).

[6] J. Berland, C. Bogey, C. Bailly, *Computers and Fluids*, **35**, 1459 (2006).